APPLICABILITY OF COBRA CONCEPT TO DETUMBLING SPACE DEBRIS OBJECTS

Thomas Peters, tpeters@gmv.com
Diego Escorial Olmos

GMV, Tres Cantos, Spain

ABSTRACT

COBRA is a contactless concept for de-tumbling and controlling the attitude of a target space debris object that exploits the torques generated on the target by the plume impingement of a thruster facing the target. The control strategy for de-tumbling is based on a switching strategy for the de-tumbling thruster and a pointing strategy for aiming the de-tumbling thruster at a specific region of the target. This control strategy has been developed in a previous internal study of the concept. This article discusses further developments of the original strategy and examines the general applicability of the COBRA concept, mainly in Active Debris removal missions in line with Cleanspace. The applicability of COBRA concept is investigated by examining several scenarios, namely, de-tumbling and attitude control of debris objects of varying configurations in terms of object geometry and mass parameters and in various initial rotation states. The main targets examined in this study are Envisat and PROBA 2.

Index Terms— *Active Debris Removal, Contactless de-tumbling, Plume impingement*

1. INTRODUCTION

Due to the intensive activities in the space during the last half century, the population of man-made space objects is playing an increasingly important role in the space environment. Today more than 6000 satellites are orbiting around the Earth but only 900 are operational and the problem is going to grow in the future: almost 1200 new satellites are expected to be launched in the next 8 years based on a forecast by Euroconsult. The population of man-made space objects consists of approximately 6% operational spacecraft, 22% non-functional spacecraft, 17% rocket upper stages, 13% mission-related debris and 42% fragments from explosions or collisions [1]. Table 1 provides a classification of the major types of debris and their characteristics. Currently, the removal of small debris objects is not practical [2]. A commonly proposed strategy consists of mitigation on one hand and removal of the largest objects on the other, which would remove the largest sources of potential new small debris. The total mass of the population is estimated at 6300 tons.

Although it is not practical to remove anything but the largest debris objects, such an approach would nevertheless make sense, because the large objects tend to be the primary source of new small debris and because 99% of the total mass of the debris is concentrated in the large objects.

Table 1: Debris classification (from [1], [3])

Type	Characteristics	Hazard
Tiny	Not tracked, <1 cm	Shielding exists, damage to satellites may occur
Small	Not tracked, diameter 1 – 10 cm, 98% of lethal objects, ~400.000 objects in LEO	Too small to track and avoid, too heavy to shield against
Medium	Tracked, diameter >10 cm, <2 kg, 2% of lethal objects, ~24.000 objects in LEO, > 99% of mass (incl. large objects)	Avoidance manoeuvres performed most often for this category
Large	Tracked, >2 kg, <1% of lethal objects, > 99% of mass (incl. medium objects)	Primary source of new small debris, 99% of collision area and mass

Many studies have recently been performed on the feasibility of removing Envisat from orbit [4], [5]. Two options that are under serious consideration are capture by means of a net capture system, and capture by means of a robotic arm. A serious complication to the removal mission is that recent measurements indicate that Envisat is spinning at a rate of 2.6 – 3.5°/s [6], [7]. This has led to the requirement that a target spin rate of 5°/s should be assumed for the removal mission of Envisat [5]. Capturing Envisat by means of a robotic arm requires a precise synchronization of the chaser with the attitude motion of Envisat, such that the chaser would remain stationary with respect to a reference frame fixed to Envisat [8]. Such a manoeuvre is both risky and fairly expensive in terms of ΔV.

In this context a contactless de-tumbling method is proposed. COBRA is a method to modify the attitude motion of a non-cooperative satellite by means of the interaction between chemical thruster exhaust gases and the target satellite. The COBRA concept was originally proposed as a method to modify the orbit of a debris object and the possibility of attitude control of the object was noted in that study [10]. Study results indicated that although orbit modification was possible, the associated ΔV cost was prohibitively expensive. Attitude control would however be feasible at a reasonable ΔV cost. A study was performed to investigate the feasibility of de-tumbling Envisat prior to capture [11], [12] and an experiment was proposed to validate the COBRA approach [13]. A control strategy for

pointing the thruster in the correct direction with respect to the target and switching it on an off was investigated for de-tumbling Envisat [14].

The advantages of the COBRA concept are the following. COBRA is a contactless method to influence the attitude of an uncooperative space object. As such, it removes or reduces the need for complicated synchronization manoeuvres (in which the chaser follows the attitude motion of the target) or complicated manipulator path planning to capture the target. The debris can first be brought into a state in which it is easier to handle by means of a capture device. Furthermore, COBRA is a method that requires very little hardware or new technology in addition to what is already required for rendezvous with space debris.

Simulation results described in a previous article [14] have shown that a simple pointing and switching strategy for COBRA can successfully de-tumble a large space object such as Envisat in a relatively short time and using only a modest amount of ΔV, namely from an initial rotation rate of 5°/s to 0.5°/s in under one orbit. These simulations assumed a relatively favourable rotation state of Envisat, which allowed pointing the thruster at the Solar panel. The normal of the Solar panel was perpendicular to the rotation axis, such that a large torque could be generated. In the current article, new simulations will be presented for less favourable rotation states of Envisat. In addition simulations will be presented for a different target, PROBA 2. PROBA 2 is a roughly cube-shaped object, which means that there is no particular geometry (location plus orientation) of the thruster with respect to target that generates high torques.

Results have indicated that the ΔV required could be improved, in part by updating the thruster layout of the chaser and in part by updating the control strategy. The control strategy is improved in a number of ways. Previous results indicated that the ΔV overhead (that is, the ΔV not directly contributing to de-tumbling the debris) was higher than expected based on the ΔV required to compensate for the activation of the de-tumbling thruster. A part of the overhead can be explained by the cosine losses, but a substantial fraction was due to attitude control. Some effort was spent to improve the pointing strategy and the attitude control of the chaser to reduce this overhead. A large effort was made to understand what is needed for an effective pointing strategy and to improve the pointing strategy. The current strategy uses a very simple model to predict the torques imparted on the target. The prediction model is improved such that the torque imparted on the target is closer to the desired torque. The updated control strategy is especially relevant for satellites that do not have an asymmetrical shape.

2. PLUME IMPINGEMENT MODELLING

The model developed for plume impingement was developed specifically for fast execution speeds. The calculation of the forces acting on the surface of the target due to plume impingement requires a discretization of the model, that is, a panel method [9]. To achieve fast calculation speeds the models for the plume and for the surface interaction were simplified to the maximum extent possible to save computation time required for the computation of complicated functions, seeing that a panel method requires evaluating these functions at every panel.

Table 2 provides the characteristics of the thruster considered for the simulations

Table 2: Thruster characteristics

Parameter	Value
Force	1 N, 5 N
Expansion ratio	80
Chamber pressure	$11 \cdot 10^5$ Pa
Chamber temperature	1200 N
Gas mixture molecular mass	10.5 g/mol

2.1 Plume model

In earlier studies [10], [11], [12], [13] of the COBRA concept, the model proposed by Fehse [15] was used to model the pressure exerted on each surface element. The validation of the Fehse model is not available in published literature [15]. Simons [16] proposed a model (derived from a model by Boynton [17]) for the thruster plume density distribution that has the following form:

$$\frac{\rho}{\rho^*} = \phi_0 \left(\frac{R^*}{r} \right)^2 f(\vartheta) \tag{1}$$

In this equation, starred quantities refer to the nozzle throat. R* is the radius of the nozzle throat, r is the distance from the origin, ϕ_0 is a thruster constant and f(ϑ) is an angular distribution function. Simons proposes the following angular distribution function:

$$f(\vartheta) = \begin{cases} \cos^{\frac{2}{\gamma-1}} \left(\frac{\pi \vartheta}{2 \vartheta_{\lim}} \right) & \vartheta <= \vartheta_0 \\ f(\vartheta_0) \cdot e^{-\beta(\vartheta - \vartheta_0)} & \vartheta > \vartheta_0 \end{cases} \tag{2}$$

Here, γ is the ratio of specific heats of the exhaust gases. The maximum angle $\vartheta_{\lim}$ is given by the maximum turn angle of the flow plus the exit angle of the thruster [18]:

$$\vartheta_{\lim} = \nu(M=\infty) - \nu(M_E) + \alpha_E \tag{3}$$

Further details on the Simons plume can be found in [16], [18], [19]. It is assumed that the gas expands to its limiting velocity throughout the plume. The limiting velocity is given by:

$$V_{\lim} = \sqrt{\frac{2\gamma}{\gamma - 1} RT_0} \tag{4}$$

The momentum carried by the plume is then given by:

$$q = \rho V_{\lim}^2 \tag{5}$$

Because the limiting velocity is assumed to be constant throughout the plume, the momentum flux as a function of the location in the plume can be determined using a modification of equation (1).

$$q = C \cdot r^{-2} f(\vartheta) \tag{6}$$

The thruster constant C is determined by considering the force balance in the direction of the thruster centre line. The thrust level of the modelled thruster is specified, and the amount of force exerted on a unit sphere must be equal to the thrust level of the thruster. The constant C can therefore be found by integrating the angular distribution function over the unit sphere:

$$C = \frac{F_{thr}}{\pi \int_0^{\pi} f(\vartheta) \sin(2\vartheta) d\vartheta} \tag{7}$$

Figure 1 shows a comparison of the density distribution function for different values of the ratio of specific heats. Also included is data from a Direct Simulation Monte Carlo [21] (DSMC) simulation performed by ESA for a hydrazine thruster plume. To approximate the DSMC data, a boundary layer thickness of 0.59% of the nozzle exit radius was assumed. The Simons model fits the DSMC data almost exactly. Also included are calculations for different values of the ratio of specific heats and calculations based on the model proposed by Fehse. Higher ratios of specific heats cause the plume to become narrower, and lower ratios of specific heats cause the plume to become wider [22]. The model by Fehse overestimates the density in the region from 30° to about 60° - 70° for a ratio of specific heats of 1.37, meaning that the plume is broader for that region.

Note that thicker boundary layers of 5 – 20% of the nozzle exit radius need to be assumed to reproduce experimental data for N2 cold gas thruster plumes from references [18] and [20]. The experimental data in these references indicates that the density is in fact lower than predicted by the first of equation (2) in a range of angles 20° to 40° from the thruster centre line for 0.5 Newton N_2 cold gas thrusters.

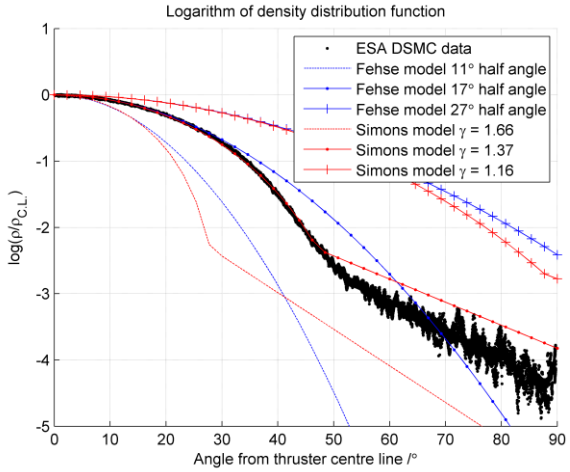

Figure 1: Comparison of density distributions functions

This appears to be caused by a non-zero displacement thickness. The Simons model assumes a displacement thickness of zero and a thin boundary layer. For larger thrusters the reduction of density with respect to the prediction of equation (2) does not occur [22].

2.2 Surface interaction model

The thruster flow is assumed to be hyperthermal; that is to say, the thermal motion of the gas is negligible compared to the speed of the flow. The average speed of a gas molecule obeying a Maxwellian distribution is given by:

$$V_{avg} = \sqrt{\frac{8}{\pi} RT} \tag{8}$$

Assuming that the expansion of the flow in the thruster isentropic [9], the gas temperature at the nozzle exit is 145 K for the thruster considered in Table 2. This leads to an average thermal velocity of 540 m/s. The limiting velocity in the far field (from equation (4)) is 2650 m/s. The average thermal velocity at the nozzle exit is about 20% of the limiting velocity. The plume expands after leaving the nozzle, causing the temperature to drop. DSMC data indicates that the temperature in the far field can be as low as 20 K, leading to an average thermal velocity of the gas that is 7.5% of the limiting velocity. This is a small, but significant fraction of the limiting velocity.

The net effect of dropping the hyperthermal flow assumption would be that gas molecules can have velocity components perpendicular to the line of sight to the thruster. For an observer travelling with the gas molecules, it is as if the gas molecules move according to a Maxwellian distribution.

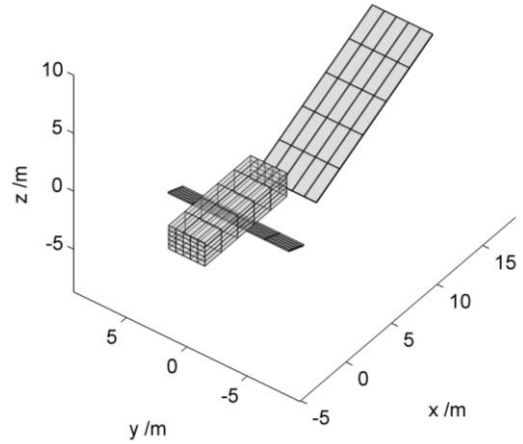

Figure 2: Envisat model discretization

In hyperthermal flow the force acting on a surface element is given by [24]:

$$d\mathbf{F} = \rho V^2 \cos\alpha \times \left\{ \left[\left(2 - \sigma_n - \sigma_t\right)\cos\alpha + \sigma_n \frac{V_w}{V} \right]\mathbf{n} + \sigma_t \mathbf{e}_V \right\} dA \tag{9}$$

In this equation, ρ is the density, V is the jet velocity, α the incidence angle of the surface element, σ_n and σ_t the normal and tangential accommodation coefficients, V_w the velocity with which fully accommodated molecules leave the surface, **n** the surface normal, $\mathbf{e}_V$ the unit vector in the direction of the velocity vector and dA the area of the surface element.

The velocity with which molecules leave the surface is given by:

$$V_w = \sqrt{\tfrac{1}{2}\pi R T_w} \tag{10}$$

If the hyperthermal assumption is dropped, then the equations for the force acting on a surface element become significantly more complicated [25], [26], such that evaluating these equations requires more computational overhead. For this reason, the hyperthermal assumption is maintained. Furthermore, it is assumed that the normal and the tangential accommodation coefficients σ_n and σ_t are equal and that the wall temperature is equal to zero. The force on a surface element is now given by:

$$d\mathbf{F} = \rho V^2 \cos\alpha \times \left\{ 2\left(1 - \sigma\right)\cos\alpha \cdot \mathbf{n} + \sigma \cdot \mathbf{e}_V \right\} dA \tag{11}$$

The value of σ is set to 97% based on the observation that 97% of ambient gas molecules are diffusely reflected by the surfaces of the target object [27].

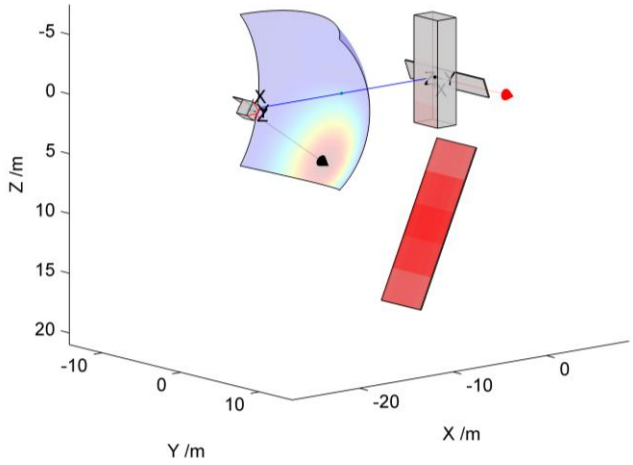

Figure 3: Torque on the target

Figure 2 shows the discretization of the Envisat model, using 5 (10 elements are used for the simulations of the controller) elements per face and 1 element for the sides of the Solar panel and the SAR antenna. All fine surface details have been removed. To compute the force and torque acting on Envisat equation (6) and (11) are evaluated at the centre of each of the panels if the panel is visible from the thruster. Visibility is calculated by determining whether the line of sight from the centre of the panel to the thruster on the chaser is obstructed by other panels.

The total force on the target object is calculated by summing (11) over all panels and the total torque by taking the cross product of the position of the centre of the panel with the force acting on the panel and summing over all panels.

3. TORQUE GENERATION

Torque generation on the target depends on two effects. First, the target object may have an asymmetric shape. In this case the chaser will impart a torque on the target even if the gas jet is directed at the centre of mass of the target. Second, the gas jet can be pointed away from the centre of mass such that the pressure distribution on the surface of the target is non-symmetrical with respect to the centre of mass, even if the target is symmetric. A combination of both techniques ensures that any object can be controlled.

Due to the geometry of the problem, the main components of the torque imparted on the target are contained in the plane perpendicular to the line of sight of the thruster to the centre of mass of the target. In Figure 3 this plane is the yz-plane of the local vertical, local horizontal frame. So, to de-spin the target the de-spinning torque needs to be contained in this perpendicular plane. This implies that the chaser needs to be positioned on a plane perpendicular to the spin axis of the target. In Figure 3 the chaser is located 20 m behind the target.

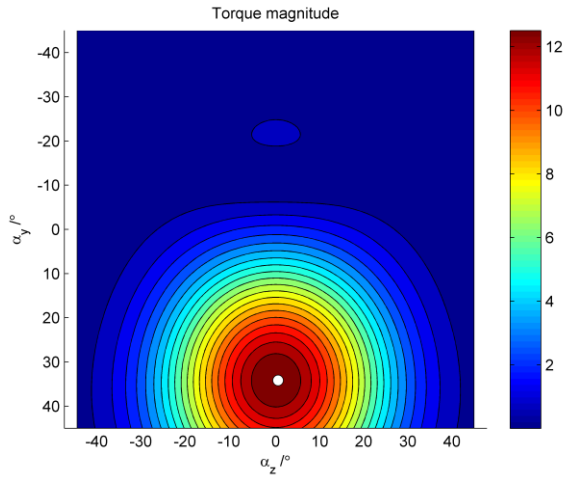

Figure 4: Torque magnitude

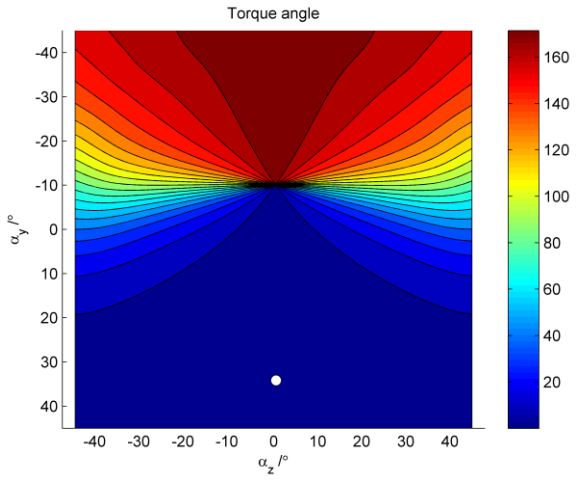

Figure 5: Torque angle

Figure 3 shows how torques can be generated by pointing the thruster at different points on the surface of the target. The pressure distribution on the target is shown in red, the chaser thrust pointing direction is shown with a black arrow, the torque on the target for the orientation of the chaser shown in the figure is represented by a red arrow and the line of sight from the chaser to the target is shown in blue. The variation in the torque that can be imparted on the target has been investigated systematically by varying the attitude of the chaser for different orientations of the target. Figure 3 shows an orientation of the target that leads to a fairly simple and symmetric graph of the torque as a function of the attitude of the chaser. The variation in the magnitude of the torque as a function of the attitude of the chaser is shown on a curved screen in front of the chaser. Blue regions indicate a low torque and red regions indicate a high torque.
To obtain this attitude grid the attitude of the chaser is varied in a 40° by 40° grid of rotations around the y and z axis using the following pointing quaternion:

$$q_s = \cos\left(\tfrac{1}{2}\alpha_m\right)$$
$$\mathbf{q}_v = \frac{\sin\left(\tfrac{1}{2}\alpha_m\right)}{\alpha_m}\begin{bmatrix}0 & \alpha_y & \alpha_z\end{bmatrix} \qquad (12)$$
$$\alpha_m = \sqrt{\alpha_y^2 + \alpha_z^2}$$

Figure 4 shows the variation of the magnitude of the torque as a function of the orientation of the chaser. The magnitude of the torque is given by:

$$T = \sqrt{\mathbf{T} \bullet \mathbf{T}} \qquad (13)$$

The maximum torque imparted on the target is of the order of 12 Nm. The thrust level used for generating this plot is 5 N, and a force of about 1 N is acting on the target.

For generating the maximum torque, the chaser points approximately to the centre of the solar panel, at a distance of about 12 m from the target centre of mass.
These results indicate that only a fraction of the plume (about 20%) is intercepted. If Envisat is rotating around the y-axis, then the chaser cannot get close to the target because the tip of the solar panel is located at a distance of about 19 m from the centre of mass. In fact, the distance of 20 m that was used to generate this example is too close to the target and for safety reasons a distance of about 25 m should be selected. This means that the torque imparted on the target will decrease.
Figure 5 shows the in-plane angle of the torque with respect to the desired torque directed along the positive y-axis. The torque angle is computed from:

$$\alpha_T = \tan^{-1}\left(\frac{T_y}{T_z}\right) \qquad (14)$$

The angle shown in Figure 5 is computed by subtracting the angle of the desired torque from the angle of the torque that is actually imparted.
The figure shows that the behaviour of the torque direction as a function of the orientation of the chaser is complicated even for the simple chaser – target geometry shown in Figure 3. In principle torques could be generated in all directions; all angles from 0 to 180° are present. However, the pole of the torque angle is not located at the line of sight direction to the target, but about 10° above it. Figure 4 shows that a maximum torque of 2 Nm could be generated in the opposite direction, at 180°, if the chaser points 20° above the line of sight.
The figure also shows that the lines for which the torque angle is constant originating from the pole are not straight, but curved. What's more, the region for which the torque

angle is approximately equal to zero actually grows when the chaser points farther away from the pole. A control strategy needs to take these facts into account.

4. CONTROL STRATEGIES

Two control strategies are under investigation for the thruster pointing and switching strategy. Both strategies rely on computing a desired torque on the target and a corresponding desired torque in the plane perpendicular to the line of sight to the chaser. The difference between the strategies lies in the way the thruster pointing is handled. In the first strategy the chaser points the thruster to a point along a line perpendicular to the desired torque. For example, in Figure 5 the direction of the desired torque is towards the right (i.e., increasing α_z), and the chaser needs to point to a downward direction (i.e., increasing α_y) to achieve this torque. The second strategy follows the contour for which the torque angle is equal to the desired torque angle and finds the maximum torque along this curve to determine the pointing direction.
The desired angular velocity is computed using proportional and derivative gain matrices:

$$\dot{\boldsymbol{\omega}}_{des} = -\mathbf{K}_P\left(\boldsymbol{\omega} - \boldsymbol{\omega}_{ref}\right) - \mathbf{K}_D\dot{\boldsymbol{\omega}} \tag{15}$$

Next, the desired torque in the target body fixed frame is computed using Euler equations.

$$\mathbf{T}_{des,bff} = \mathbf{I}\dot{\boldsymbol{\omega}}_{des,bff} + \boldsymbol{\omega}_{bff} \times \left(\mathbf{I}\boldsymbol{\omega}_{bff}\right) \tag{16}$$

Finally, the torque is transformed from the body fixed frame to the local vertical, local horizontal frame.

4.1 Strategy 1

As stated, the first strategy calculates a line of desired force application after computing the desired torque on the target. The line of force application is perpendicular to the line of sight to the target, and perpendicular to the desired torque. A direction vector along this line can be found as:

$$\mathbf{u}_{des} = \frac{-\mathbf{r}_{chs} \times \mathbf{T}_{des}}{\left\|\mathbf{r}_{chs} \times \mathbf{T}_{des}\right\|} \tag{17}$$

Next, the chaser computes the maximum possible off-centre angle that ensures that a large fraction of the plume is intercepted. Figure 6 illustrates this idea. The unit vector along the desired torque direction is shown in blue, the direction vector from the chaser to the target in black, and the direction vector along the line of force application is shown in black. The face centres of the discretized model are analysed and those centres that lie within 10° of the desired line of force application are retained. These are the red dots shown in the figure. A distance in between the average and maximum distance of these points to the target centre of mass is used to compute the desired off-centre angle.

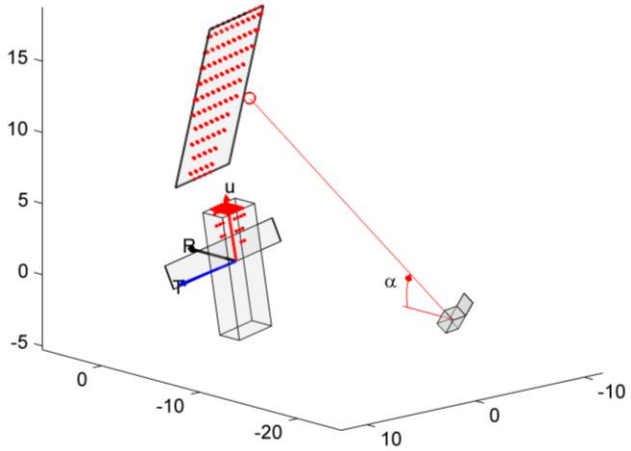

Figure 6: Calculation of the off-centre angle

A lower limit is set to the off-centre angle such that the chaser never points the thruster close to the line of sight. The thruster is switched on when the following conditions are satisfied: the off-centre angle needs to be larger than the lower limit, and the desired torque needs to be perpendicular to the line of sight from the chaser to the target by some margin. A more detailed description of the strategy is available in [14].

4.2 Strategy 2

The second strategy uses a torque prediction model using a simpler model of the target geometry (in this case, using fewer panels and no shadowing computations) to predict the torque on the target as a function of the pointing direction. This model is used to find and track the maximum torque along the curve of the desired torque direction.
The strategy works by at each time step numerically computing the current torque and the first and second derivatives of the torque with respect to magnitude and angle. This requires 7 evaluations of the plume impingement model per time step.
The algorithm then takes a step in the angles α_y and α_z that takes the torque angle closer to the desired torque angle. Referring to Figure 5, this step is perpendicular to the black lines separating the coloured regions. Some care must be taken when these curves have a high curvature, because this could lead the angles α_y and α_z to become unacceptably large. This situation is remedied by taking a step along the current curve of constant torque angle towards the pole. This ensures that the angles α_y and α_z remain small – the pole is always fairly close to the direction to the target.

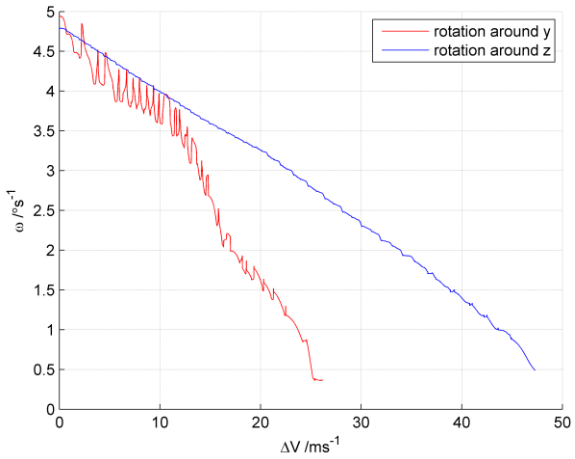

Figure 7: Envisat detumbling; strategy 1

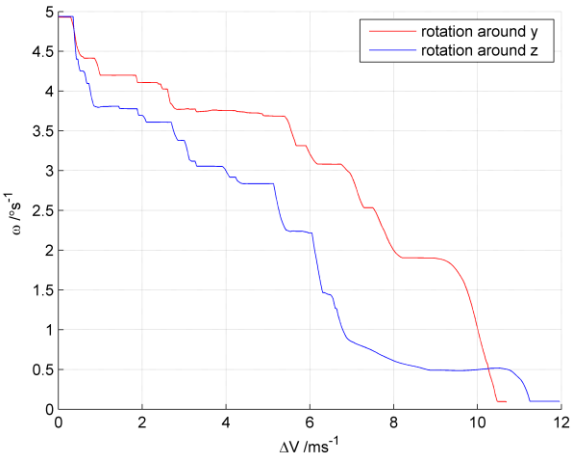

Figure 8: PROBA2 Detumbling, strategy 2

As the correct torque angle is reached, the algorithm steps along the curve of constant torque angle in the direction of the maximum torque. The algorithm takes only one step in the angles α_y and α_z per time step of the simulation to reduce computational load. This means that the algorithm requires a number of time steps before it finds and starts tracking the maximum torque. The thruster switching strategy takes this into account by only switching on the de-tumbling thruster when the difference between the estimated torque associated with the current pointing direction and the desired torque is smaller than a certain margin.

Finally, an optional module is included to control the position of the chaser to remain at a point at a fixed distance perpendicular to the target rotation vector. This point is found by intersecting the plane perpendicular to the target rotation vector with the xy-plane of the local vertical, local horizontal frame and choosing the point closest to the chaser current location.

5. SIMULATION RESULTS

5.1 Envisat

For the Envisat simulations the chaser is located at a distance of 23 m from the target in these simulations. Figure 7 shows the results of two de-tumbling scenarios for Envisat, namely, rotation around the body y-axis and rotation around the body z-axis. Of these two, the rotation around the body z-axis is the less desirable case, because the solar panel is seen from the side, meaning that the surface visible from the thruster is much smaller. It should be noted that the rotation state of Envisat around the y-axis is not stable and a large nutation is present, meaning that the angular velocity vector moves between the body y- and z-axes.

This explains the sudden shift in deceleration speed in Figure 7. At this point the solar panel becomes visible head on at the appropriate orientation of the target and the de-spinning becomes more efficient. The rotation around the z-axis is stable, such that the decrease in the rotation rate is much more orderly. The total ΔV required is 25 m/s for the rotation around y and 47 m/s for the rotation around z. The total time is between 100 minutes for the rotation around y and 150 minutes for the rotation around z.

5.2 PROBA2

For PROBA2 strategy 1 did not lead to good results because of the nearly symmetrical body of PROBA2. Figure 9 shows a sketch of the initial conditions. The thrust of the thruster was scaled down to 1 N and the chaser was put at a distance of 6 m. The minimum off-centre angle was set to about 5° instead of 19° for Envisat, but still the thruster never switched on.

The second strategy was created to remedy this situation. Figure 9 shows the results for two different rotation scenarios, both leading to a de-spinning to below 0.1 °/s at a cost of about 11 m/s. For the rotation case around z it is apparent that at a rotation speed of 0.5 °/s the chaser spends a lot of ΔV without changing the rotation state of the target by a very great amount. In this region the desired pointing direction shifts fairly rapidly and the chaser performs fast attitude motion to track the desired pointing direction.

6. DISCUSSION

The development of the plume model has focused on execution speed, and several important simplifying assumptions have been made. It is expected that the assumptions on the gas - surface interaction may have some impact on the torque experienced by the target.

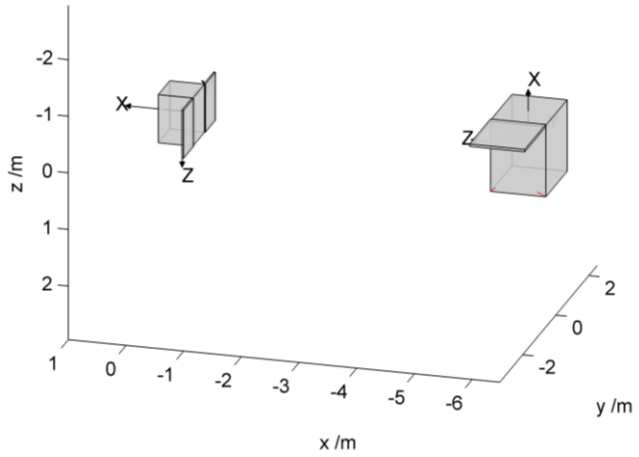

Figure 9: PROBA2 (left) and chaser (right)

In addition, the discretization of the target model is fairly coarse and does not include surface detail (such as instrumentation, antennas, etc.). On the other hand, it is expected that the qualitative behaviour remains the same.

Some advances have been made in the understanding of the plume model with respect to [14]. There, it was assumed that the ratio of specific heats of the exhaust gases was about 1.28, while the true value should be 1.37. The suggestion to narrow the plume by using a noble gas with a specific heat of 1.66 is still valid. Current results indicate that this could narrow the width of the isentropic core of the plume by 30°. It may also be possible to generate a narrower plume by choosing a different nozzle geometry with a smaller divergence angle at the nozzle exit. On the other hand, reference [20] indicates that for small cold gas thrusters the effect of the boundary layer on the nozzle flow is quite large, and that the boundary layer effect may lead to a slightly narrower (~5°) core of the plume. Simulation results have shown that narrow plumes lead to dramatic improvements in de-tumbling performance.

For a COBRA style de-tumbling a narrow plume is desirable, because it means that the chaser can stay at a larger distance to generate the same force on the target object. In addition, because the plume is narrower, the plume pointing can be used more effectively for attitude control of the debris object. If there is only a small variation of pressure with respect to the angle from the bore sight, then the pressure distribution on the target will be relatively uniform. On the other hand, if the plume is narrow, then the pressure distribution on the target becomes more sensitive to the pointing of the thruster, which increases the potential to generate torques on the target and therefore the potential to exert attitude control over the target.

The first strategy for controlling the attitude of a target debris object depends to an extent on the fact that the target has an asymmetric shape. This is reflected in the fact that a minimum off-centre angle is used that effectively ensures that the chaser only performs thrusts when it points to the solar panel. It was found that the first strategy does not work for nearly symmetrical objects. It is suspected that the calculation of the off-centre angle leads to angles that are always smaller than the minimum off-centre angle. The calculation of the desired line of force application in equation (17) cannot take into account the fact that the pole of the rotation may not be located exactly along the direction to the target; see Figure 6: the pole of rotation is 10° above the line of sight to the target. It is suspected that for a nearly symmetrical target object the torque angle as a function of the pointing angles is fairly simple for all target orientations. It may therefore be possible to use strategy 1 with a fixed off-centre angle.

The results for the second strategy indicate that it is possible to de-tumble an object that does not have a pronounced asymmetry such as Envisat. In fact, the absence of the asymmetry allows the chaser to move much closer to the target, which increases the force that can be imparted. The second strategy is computationally more expensive than strategy 1, such that it would be desirable to adapt strategy 1 in such a way that it is applicable to symmetric targets.

Finally, the second strategy is better able to reduce the angular velocity of the target when the angular velocity of the target is already below about 0.5 °/s. This means that a hybrid approach may be desirable. Strategy 1 could be used for the initial de-spinning to about 0.5 - 1 °/s and strategy 2 to reduce the angular velocity to below 0.1 °/s.

7. CONCLUSIONS

COBRA, or de-tumbling satellites by means of plume impingement, has been shown to be a promising technique for de-tumbling space debris objects. The technique does not require additional equipment on the chaser apart from the equipment already there for performing rendezvous with the object.

Ongoing investigations have improved the plume model and have provided a more realistic (albeit highly simplified) model of the surface interaction of the plume exhaust gases with the surface of the target object.

Simulations have shown that de-tumbling by means of plume impingements is possible even if the target object is in an unfavourable rotation state and even for satellites that do not have a pronounced asymmetrical shape.

8. REFERENCES

[1] Committee on Space Debris, 1995, Orbital Debris: A Technical Assessment, National Academies Press

[2] Kaplan, M. H., Bradley Boone, B., Brown, R., Criss, T. B., Tunstel, E. W., 2010, Engineering Issues for All

Major Modes of In Situ Space Debris Capture, AIAA SPACE 2010 Conference & Exposition 30 August - 2 September 2010, Anaheim, California

[3] Levin, E., Pearson, J., Carroll, J., "Wholesale Debris Removal From LEO," Acta Astronautica, v. 73, pp. 100-108,. April-May 2012.

[4] ESA, 2012, CDF report eDeorbit, CDF-135(C)

[5] ESA eDeorbit study team, 2015, e.deorbit Phase B1 - Mission & System Requirements Document (MSRD)

[6] Bastida Virgili, B., Lemmens, S., Krag, H., 2014, Investigation on Envisat attitude motion, e.Deorbit Workshop,

[7] Kucharski, D., Kirchner, G., Koidl, F., Fan, C., Carman, R., Moore, C., Feng, Q., 2014, "Attitude and Spin Period of Space Debris Envisat Measured by Satellite Laser Ranging", IEEE Transactions on Geoscience and Remote Sensing, Vol. 52 , Issue 12, pp. 7651 – 7657, DOI 10.1109/TGRS.2014.2316138

[8] Airbus Defence and Space, 2014, e.Deorbit Mission Phase A final report, EDEORBIT-ASD-RP-0009

[9] Anderson, J. D., 1991, "Fundamentals of Aerodynamics," McGraw-Hill

[10] Peters, T. V., Pellacani, A., Attina, P., Lavagna, M., Benvenuto, R., Luraschi, E., "Cobra Active Debris Removal Concept", IAC-13-A6,6,6, Proceedings of the 64th International Astronautical Congress, Beijing, 2013

[11] Ferrari, F., Benvenuto, R., Lavagna, M., 2014, "Gas Plume Impingement Technique For Space Debris De-Tumbling," Proceedings of the 9th International ESA Conference on Guidance, Navigation & Control Systems (GNC 2014)

[12] Ferrari, F., Lavagna, M., 2015, "Free Tumbling Objects Attitude Control Via Contactless Chaser Authority Exploiting a Formation Flying Architecture", Proceedings of the 8th International Workshop on Satellite Constellations and Formation Flying, Delft, The Netherlands

[13] Peters, T. V., Escorial Olmos, D., Pellacani, A., Avilés Rodrigálvarez, M., Lavagna, M., Ferrari, F., Attina, P., Parissenti, G., Cropp, A., "The COBRA IRIDES experiment," IAC-14-A6.6.9, Proceedings of the 65th International Astronautical Congress, Toronto, 2014

[14] Peters, T. V., Escorial Olmos, D., 2015, "Cobra Contactless De-Tumbling, " Proceedings of the 5th CEAS Air and Space Conference

[15] Fehse, W., Automated Rendezvous and Docking of Spacecraft, Cambridge University Press, New York, 2003

[16] Simons, G. A., "Effect of Nozzle Boundary Layers on Rocket Exhaust Plumes", AIAA Journal, vol. 10, issue 11, 1972, pp. 1534-1535 doi: 10.2514/3.6656

[17] Boynton, F. P., 1967, "Highly Underexpanded Jet Structure: Exact and Approximate Calculations," AIAA Journal, Vol. 5, No. 9, Sept. 1967, pp. 1703-1704.

[18] Legge, H., Boetcher, R. D., 1985, "Modelling control thruster plume flow and impingement," Proceedings of the 13th International Symposium on Rarefied Gas Dynamics, pp. 983-992

[19] Boyd, I.D., 1988, "Modelling of Satellite Control Thruster Plumes," PhD Thesis, University of Southampton

[20] Plähn, K., Dettleff, G., 2001, "Modelling of N2-thruster plumes based on experiments in STG," Rarefied Gas Dynamics: 22nd International Symposium, Vol. 585. No. 1.

[21] Bird, G. A., 1994, "Molecular Gas Dynamics and the Direct Simulation of Gas Flows," Claredon, Oxford

[22] Dettleff, G., 1991, "Plume flow and plume impingement in space technology," Progress in Aerospace Sciences, Vol. 28, issue 1, pp. 1-71, doi: 10.1016/0376-0421(91)90008-R

[23] Boynton, F. P., 1968, "Exhaust plumes from nozzles with wall boundary layers." Journal of Spacecraft and Rockets, Vol. 5, No. 10, pp. 1143-1147, doi: 10.2514/3.29439

[24] Storch, J. A., 2002, Aerodynamic Disturbances on Spacecraft in Free-Molecular Flow, TR-2003(3397)-1

[25] Fuller, J. D., Tolson, R. H., 2009, "Improved Method for the Estimation of Spacecraft Free-Molecular Aerodynamic Properties", Journal of Spacecraft and Rockets, Vol. 46, No. 5, pp. 938-948, doi: 10.2514/1.43205

[26] Schaaf, S. A., Chambre, P. L., 1958, "Flow of Rarefied Gases," Fundamentals of Gas Dynamics, edited by H. W. Emmons, Princeton Univ. Press, Princeton, NJ, pp. 687–708.

[27] Moe K., Moe M. M., 2005, "Gas–surface interactions and satellite drag coefficients", Planetary and Space Science 53 (2005), pp. 793–801